ARTICLE OPEN

The histone methyltransferase EZH2 primes the early differentiation of follicular helper T cells during acute viral infection

Xiangyu Chen[1], Guoshuai Cao[2], Jialin Wu[1], Xinxin Wang[3], Zhiwei Pan[1], Jianbao Gao[3], Qin Tian[1], Lifan Xu[1], Zhirong Li[1], Yaxing Hao[1], Qizhao Huang[4], Pengcheng Wang[1], Minglu Xiao[1], Luoyingzi Xie[1], Shupei Tang[1], Zhenyu Liu[1], Li Hu[1], Jianfang Tang[1], Ran He[1], Li Wang[1], Xinyuan Zhou[1], Yuzhang Wu[1], Mengjie Chen[5], Beicheng Sun[6], Bo Zhu[3], Jun Huang[2] and Lilin Ye[1]

Epigenetic modifications to histones dictate the differentiation of naïve CD4$^+$ T cells into different subsets of effector T helper (T_H) cells. The histone methyltransferase enhancer of zeste homolog 2 (EZH2) has been implicated in the mechanism regulating the differentiation of T_H1, T_H2 and regulatory T (T_{reg}) cells. However, whether and how EZH2 regulates follicular helper T (T_{FH}) cell differentiation remain unknown. Using a mouse model of acute lymphocytic choriomeningitis virus (LCMV) infection, we observed abundant EZH2 expression and associated H3K27me3 modifications preferentially in the early committed virus-specific T_{FH} cells compared to those in T_H1 cells. Ablation of EZH2 in LCMV-specific CD4$^+$ T cells leads to a selective impairment of early T_{FH} cell fate commitment, but not late T_{FH} differentiation or memory T_{FH} maintenance. Mechanistically, EZH2 specifically stabilizes the chromatin accessibility of a cluster of genes that are important for T_{FH} fate commitment, particularly *B cell lymphoma 6 (Bcl6)*, and thus directs T_{FH} cell commitment. Therefore, we identified the chromatin-modifying enzyme EZH2 as a novel regulator of early T_{FH} differentiation during acute viral infection.

Cellular & Molecular Immunology (2020) 17:247–260; https://doi.org/10.1038/s41423-019-0219-z

INTRODUCTION

During pathogenic infections, follicular T helper (T_{FH}) cells provide essential assistance to cognate pathogen-specific B cells that enable them to initiate and sustain germinal center (GC) reactions in B-cell follicles within secondary lymphoid tissues.[1] GC reactions lead to both the rapid production of high-affinity antibodies that protect against the immediate infection and the subsequent generation of persistent humoral immune memory for long-term protection.[1,2] In the early stage of GC reactions, intimate interactions between early differentiated T_{FH} cells and newly activated cognate B cells in the interfollicular regions of secondary lymphoid tissues direct the migration of both cell types to B-cell follicles, in turn cooperating to prime early GC responses.[3] During ongoing GC reactions, T_{FH} cells promote the survival, proliferation, class switching and hypermutation of cognate B cells and eventually drive them to differentiate into long-lived memory B cells and antibody-secreting plasma cells by secreting important cytokines such as IL-21,[4] IL-4[5] and IL-9[6] and engaging certain cell surface-bound receptors and their matching ligands, including CD40-CD40L,[7] ICOS-ICOSL[7] and PD-1-PD-L1.[8] Unlike other lineages of CD4$^+$ helper T (T_H) cells, T_{FH} cells are programmed to express the chemokine receptor CXCR5.[9–11] In response to the chemoattractant CXCL3,[12,13] CXCR5$^+$ T_{FH} cells migrate to B-cell follicles, where they physically interact with cognate B cells.[1]

Given the critical role of T_{FH} cells in B-cell-mediated humoral immunity, investigations of the early fate commitment of T_{FH} cells are very important, as the differentiation of T_{FH} cells occurs within 48 h after acute viral infections.[14,15] The transcriptional repressor B cell lymphoma-6 (Bcl-6) functions as a "master regulator" to govern early T_{FH} cell differentiation.[16–18] A rapid induction of Bcl-6 expression in de novo activated virus-specific CD4$^+$ T cells represents a key step toward the T_{FH} fate commitment. A wide variety of transcription factors (TFs) have recently been shown to regulate Bcl-6 expression during T_{FH} differentiation.[3] STAT family TFs, including STAT1,[19] STAT3[20] and STAT4,[21] promote Bcl-6 expression in response to stimulation with the corresponding cytokines, such as IL-6, IL-12 and IL-21. Batf,[22] IRF4,[23] Notch1 and Notch2[24] have also been reported to induce Bcl-6 expression and promote T_{FH} differentiation. In contrast, the TFs Blimp-1[16] and Foxo1[25] inhibit Bcl-6 expression and subsequently repress T_{FH} differentiation. Despite the known positive and negative effects of these TFs on Bcl-6 expression, researchers have not conclusively determined whether these regulators exert their effects during the early stage of T_{FH} commitment. Transcription factor-1 (TCF-1) initiates the T_{FH} fate commitment by directly inducing Bcl-6

[1]Institute of Immunology, PLA, Third Military Medical University, 400038 Chongqing, China; [2]Institute for Molecular Engineering, University of Chicago, Chicago, IL 60637, USA; [3]Institute of Cancer, Xinqiao Hospital, Third Military Medical University, 400038 Chongqing, China; [4]Cancer Center, The General Hospital of Western Theater Command, Chengdu, China; [5]Section of Genetic Medicine, Department of Medicine, University of Chicago, Chicago, IL 60637, USA and [6]Department of Hepatobiliary Surgery, The Affiliated Drum Tower Hospital of Nanjing University Medical School, Nanjing 210009 Jiangsu, China
Correspondence: Bo Zhu (bo.zhu@tmmu.edu.cn) or Jun Huang (huangjun@uchicago.edu) or Lilin Ye (yelilinlcmv@tmmu.edu.cn)
These authors contributed equally: Xiangyu Chen, Guoshuai Cao, Jialin Wu, Xinxin Wang.

Received: 14 February 2019 Revised: 17 February 2019 Accepted: 17 February 2019
Published online: 6 March 2019

expression and suppressing Blimp-1 expression during an acute viral infection.[15,26,27] Although TCF-1 is expressed at high levels in naïve $CD4^+$ T cells,[28] activated virus-specific $CD4^+$ T cells must further increase TCF-1 expression levels for subsequent T_{FH} conversion following an acute viral infection.[15] Currently, additional factors that are responsible for the early induction of the fate commitment of T_{FH} cells remain to be determined.

Epigenetic modifications of histones have been extensively implicated in the mechanisms regulating T cell differentiation.[29,30] The epigenetic regulator enhancer of zeste homolog 2 (EZH2), which is the catalytic subunit of polycomb repressive complex 2 (PRC2), functions as a methyltransferase to induce the trimethylation of histone H3 at lysine 27.[31,32] The resulting H3K27me3 protein recruits chromatin-compressing protein complexes to certain loci to silence the expression of corresponding genes.[31,32] EZH2-mediated H3K27me3 plays a critical role in the differentiation and lineage stability of various types of $CD4^+$ T_H cells, including T_H1, T_H2 and regulatory T (T_{reg}) cells.[33–38] In the T_H1 and T_H2 lineages, several groups reported that EZH2 and the associated H3K27me3 directly bind to *Tbx21*[36,38] (which encodes the TF T-bet, a master regulator of T_H1 differentiation) and *Gata3*[36] (encoding the TF Gata3, which specifies T_H2 differentiation) to inhibit the transcription of both TFs and eventually suppress the differentiation of naïve $CD4^+$ T cells into both T_H1 and T_H2 cells. Additionally, EZH2 and H3K27me3 inhibit the differentiation of T_H1 and T_H2 cells through the direct epigenetic marking and silencing of genes that encode lineage-specific cytokines, such as *Ifng*[36,38] and *Il13*.[36,38] Paradoxically, EZH2 also induces T_H1 cell differentiation by increasing the stability of T-bet and inducing the production of T_H1 cytokines.[34,35] In T_{reg} cells, CD28-induced EZH2 expression promotes H3K27me3 deposition at gene loci that are normally repressed in Treg cells and thus plays an important role in stabilizing the lineage specification of activated T_{reg} cells.[33] Despite the profound effects of EZH2 on T_H1, T_H2 and T_{reg} differentiation, whether and how EZH2 regulates the T_{FH} fate commitment remains to be investigated.

Here, we first defined a strict lineage-specific mode of chromatin accessibility in virus-specific T_{FH} cells compared to virus-specific T_H1 cells in response to an acute infection. Bona fide differentiated virus-specific T_{FH} cells exhibited increased EZH2 expression and the associated H3K27me3 modification compared to naïve T cells and T_H1 cells in the early days after an acute lymphocytic choriomeningitis virus (LCMV) infection. Furthermore, EZH2 was required for governing the chromatin accessibility of a cluster of T_{FH}-lineage-associated genes, particularly *Bcl6*, which are essential for T_{FH} fate commitment. Accordingly, inactivation of EZH2 in virus-specific $CD4^+$ T cells led to a pronounced reduction in the early commitment but not late differentiation or maintenance of T_{FH} cells.

MATERIALS AND METHODS

Mice, virus, bacteria and tamoxifen treatment

$CD45.1^+$ SMARTA mice were a gift from Dr. R. Ahmed (Atlanta, USA). The *Ezh2*$^{fl/fl}$, *Cd4*-Cre transgenic, ERT2-Cre transgenic and C57BL/6J (CD45.1 and CD45.2) mice were obtained from Jackson Laboratories. The LCMV Armstrong strain was provided by Dr. R. Ahmed (Atlanta, USA), and 2×10^5 plaque-forming units (PFUs) of this strain were intraperitoneally injected into mice to establish an acute viral infection. *Listeria monocytogenes* expressing the LCMV glycoprotein-specific I-A^b-restricted $CD4^+$ T cell epitope GP61–80 (LM-GP61) was created from a vector strain,[39] and 1×10^7 colony-forming units (CFUs) of the recombinant bacteria were intravenously injected to establish a bacterial infection in mice. Six- to ten-week old mice of both sexes were infected without randomization or "blinding". Bone marrow (BM) chimera mice were infected 2 months after reconstitution. Tamoxifen (T5648; Sigma-Aldrich; 10 mg/ml) in sunflower oil (S5007; Sigma-Aldrich) was intraperitoneally injected into mice at a daily dose of 1 mg/mouse for 4 days. Infected mice were housed in accordance with the institutional biosafety regulations of the Third Military Medical University. All mouse experiments were performed according to the guidelines of the Institutional Animal Care and Use Committees of the Third Military Medical University.

ATAC-Seq library preparation

The ATAC-Seq libraries were prepared as previously described.[40] Briefly, 50,000 target cells were washed with PBS and then treated with lysis buffer, followed by labeling with the Nextera enzyme (15027865; Illumina). The labeled samples were immediately amplified by 9–10 cycles of polymerase chain reaction (PCR) with barcoded primers and sequenced with a HiSeq4000 instrument in a 150 bp/150 bp paired-end run or a NextSeq500 instrument in a 76 bp/76 bp paired-end run.

ATAC-Seq data preprocessing

Raw sequencing reads were first trimmed of adapters to improve the quality using Trim Galore! v0.4.4 (https://www.bioinformatics.babraham.ac.uk/projects/trim_galore/), which is a wrapper based on CutAdapt v1.14 (ref. [41]) and FastQC v0.11.5 (https://www.bioinformatics.babraham.ac.uk/projects/fastqc/). Paired-end reads that passed quality control (QC) were then aligned to mm10 using Bowtie2 v2.2.9 (ref. [42]). The resulting BAM files were then filtered again to remove unmapped reads, mate-unmapped reads, nonprimary aligned reads, reads that failed platform quality checks and PCR duplicate reads using SAMtools v1.4.1 (ref. [43]) (-F 1804). In addition, reads mapped to ChrM were also removed and PCR duplicate reads were further identified and removed using Picard v2.16.0 MarkDuplicate (https://broadinstitute.github.io/picard/).

The insert size distributions were then calculated using Picard v2.16.0 CollectInsertSizeMetrics. Since Tn5 transposase binds as a dimer and inserts two adaptors separated by 9 bp,[44] all aligned reads were shifted by + 4 bp on the positive strand and −5 bp on the negative strand using deepTools v2.5.2 alignmentSieve.[45] Afterward, peak calling was performed using MACS2 v2.1.1,[46] with a *q*-value threshold of 0.01. Peaks that overlapped with the Encode black list regions were then removed using bedtools intersect v2.26.0 (ref. [47]). We then merged peaks from all replicates and filtered peaks that are not reproducible, based on the Irreproducible Discovery Rate (IDR)[48] (IDR < 0.005), across at least one pair of replicates in each sample group. Subsequently, depending on the comparisons required for different purposes, filtered peaks from multiple sample groups were merged using the bedtools v2.26.0 merge algorithm to create genome-wide atlas of accessible chromatin regions for further analysis.

Assignment of ATAC-Seq peaks to genes

Each ATAC-Seq peak was uniquely assigned to a gene, with the corresponding feature annotations (e.g., exon, intron and intergenic) in R v3.4.1 using ChipPeakAnno v3.10.2,[49] with TxDb.Mmusculus.UCSC.mm10.knownGene v3.4.0 as the reference database. The following rules listed in order of priority were used for assignment: peaks that overlap with the transcribed region of a gene or within 2 kb upstream or downstream of the transcribed region are assigned to that gene; any remaining peaks are assigned to the nearest gene based on the distance from the center of the peak to the transcription start site (TSS) or 3′ end of the transcribed region. Regions within 5 kb of the TSS are defined as the promoter regions.

Differential peak analysis and principal component analysis

For each analysis that compares data from multiple sample groups, all required shifted BAM files from all replicates of those samples were used to generate an accessibility matrix by counting the normalized reads (normalized by DESeq2-calculated size

factors) within each peak region of the corresponding atlas peak file using deepTools v.2.5.4 multiBamSummary in BED-mode. The resulting matrix was input to DESeq2 v1.16.1 (ref. [50]) to calculate the differential accessibility of the peaks of the relevant pairs. Principal component analysis (PCA) plots were then generated using DESeq2 v1.16.1.

Coverage plots and chromatin accessibility heat map
For each sample group, shifted and RPM normalized bam files were first converted to bedgraph files by counting the normalized reads in 10 bp bins and removing reads in the Encode blacklisted regions. Then, reads obtained from replicates of the same sample group were pooled using bedtools v2.26.0 unionbedg, and the resulting merged bedgraph files were used to generate a single coverage plot for each sample group, which was visualized in IGV v2.4.4 (ref. [51]) and used to generate the chromatin accessibility heat map. Using deepTools v2.5.4 computeMatrix, each atlas peak was extended to a ±1 kb region from the peak center, and the reads from the final coverage plot were then separated into 10 bp bins to be represented as a row in the heat map. Selected differential peaks were then stacked together to generate the overall heat map using deepTools v2.5.4 plotHeatmap. Bins with read counts greater than a threshold, which was defined as the 75th percentile $+1.5\times$ inter quartile range (IQR), were capped at that threshold value to increase the visibility of low-signal regions. Capping was only performed to plot the heat map, and all other analyses were performed with uncapped values.

Flow cytometry and antibodies
Flow cytometry data were obtained with a FACSCanto II instrument (BD Biosciences) and analyzed using FlowJo software (Tree Star). The major histocompatibility complex (MHC) class II ($I\text{-}A^b$) tetramer of LCMV epitope of GP66–77 was provided by Dr. Rafi Ahmed (Emory University). The antibodies and reagents used for flow cytometry are listed in Supplementary Table 3. CXCR5 staining has been described previously.[15] Surface staining was performed in PBS containing 2% fetal bovine serum (wt/vol) on ice. Intracellular staining of Foxp3, EZH2, H3K27me3, TCF-1 and Bcl-6 was performed using the Foxp3/Transcription Factor Staining Buffer Set (00–5523; eBioscience). MHC II GP66–77 tetramer staining was performed by incubating cells with the tetramer for 1 h at 37 °C.

Immunofluorescence staining
Immunofluorescence staining was performed using previously described methods.[52] Briefly, frozen sections of the spleen were fixed with cold acetone for 10 min at 4 °C and blocked with 5% normal goat serum for 30 min. Sections were then stained with biotin-conjugated PNA (RL-1072; Vector), Alexa Fluor 647-conjugated IgD (11–26c.2a; eBioscience) and PE-conjugated CD4 (RM4–5; BD Biosciences) antibodies, followed by Alexa Fluor 488-conjugated streptavidin (25–4317–82; Invitrogen). Cover slips on which both types of cells were cultured were mounted on slides with the ProLong Antifade Kit (P-7481; Life Technologies) and examined under a Zeiss LSM 510 confocal fluorescence microscope. The images were processed with ImageJ software.

Retroviral constructs and transduction
The sequences encoding the codon-improved Cre (iCre) gene or *Bcl6* were amplified and cloned into the vector MIGR1 (MSCV-IRES-GFP) or MIGR2 (MSCV-IRES-hCD2), respectively. Retroviruses were packaged by transfecting 293T cells with the retroviral vectors along with the pCL^{eco} plasmid. SMARTA cells were activated in vivo by injecting 200 μg of the GP61–77 peptide into SMARTA mice. Eighteen hours later, activated SMARTA cells were purified and "spin-infected" by centrifugation (800 g) with retrovirus supernatants, 20 ng/ml IL-2 (130–098–221; Miltenyi Biotec) and 8 μg/ml polybrene (H9268; Sigma-Aldrich) at 37 °C for 90 min. SMARTA cells were then transferred into recipient mice, followed by the infection of the hosts with LCMV Armstrong.

Adoptive transfer
A total of 5×10^5 (for analysis on days 2, 3 or 5) or 1×10^4 (for analysis on day 8 or later) $CD45.1^+$ SMARTA cells (naïve or retrovirus-transduced) were adoptively transferred into $CD45.2^+$ recipients. On the following day, the recipients were intraperitoneally injected with 1×10^6 PFUs of LCMV Armstrong (day 2 or 5) or 1×10^7 CFUs of LM-GP66 (day 3) or were intraperitoneally injected with 2×10^5 PFUs of LCMV Armstrong (day 8 or later). For the EPZ6438-treated SMARTA cell transfer experiment, naïve $CD45.1^+$ SMARTA cells were treated with EPZ6438 (2 μM; E-7438, Active Biochem) or vehicle at 37 °C for 3 days, and then transferred into $CD45.2^+$ recipient mice, followed by infection with LCMV Armstrong.

BM chimeras
A total of 2×10^6 BM cells harvested from *Ezh2*$^{fl/fl}$ERT2-Cre ($CD45.2^+$) mice and C57BL/6J wild-type (WT) ($CD45.1^+$) mice were mixed at a ratio of 4:6. Mixed BM cells were then intravenously injected into lethally irradiated (two doses of 550 rads each) $CD45.1^+$ WT recipients. After a 2-month reconstitution, the recipient mice were infected with LCMV Armstrong.

ELISA
The LCMV-specific serum IgG titers were measured using an ELISA, as previously described.[53,54] Briefly, plates were coated with LCMV-infected cell lysates, and LCMV-specific antibodies were detected with HRP-conjugated goat anti-mouse IgG secondary antibodies (Southern Biotech).

Microarray
T_{FH} cells were isolated using a previously described method.[15] Briefly, total splenocytes obtained from WT and *Ezh2*$^{fl/fl}$*Cd4*-Cre mice on day 8 after LCMV Armstrong infection were subjected to the depletion of lineage marker-positive cells (Lin^+ cells) using biotin-conjugated antibodies (anti-B220 (RA3–6B2), anti-CD8 (53.6.7), anti-CD11c (N418), anti-TER-119 (TER-119) and anti-NK1.1 (PK136); all from BioLegend), followed by coupling to BeaverBeads Mag500 Streptavidin (22302; Beaver). The enriched Lin^- cells were then stained with anti-CD4, anti-CD44, anti-GITR, anti-CD25 and anti-CXCR5 antibodies (all identified in Supplementary Table 3). The $CD4^+CD25^-GITR^-CD44^+CXCR5^+$ T_{FH} cells were sorted with a FACS Aria II cell sorter (BD Biosciences) and then immediately lysed with TRIzol LS reagent (10296; Life Technologies). Then, total RNA was extracted and submitted to CapitalBio for a microarray analysis.

Quantitative reverse-transcription PCR
Sorted T_{FH} cells were sorted directly into TRIzol LS reagent (10296; Life Technologies). Total RNA was extracted and reverse transcribed with the RevertAid Minus First Strand cDNA Synthesis Kit (K1632; Thermo Scientific). The relative expression of various genes was determined using AceQ qPCR SYBR Green Master Mix (Q111; Vazyme) with a CFX96 Touch Real-Time System (Bio-Rad). The primers for the indicated genes are summarized in Supplementary Table 4.

ChIP
ChIP assays of sorted T_{FH} cells, T_H1 cells and naïve $CD4^+$ T cells were performed using a Simple Enzymatic Chromatin IP Kit (Magnetic Beads) (9003; Cell Signaling Technology). The resulting chromatin fragments were immunoprecipitated with an anti-H3K27me3 antibody (9733; Cell Signaling Technology), followed by binding to ChIP Grade Protein G Magnetic Beads (9006; Cell Signaling Technology) and purification with a PCR purification kit (28104; Qiagen). Sequence-indexed libraries were prepared from

immunoprecipitated chromatin fragments using the Illumina TruSeq indexed pair-ended DNA library preparation protocol and ultimately sequenced using the NextSeq500 platform.

ChIP-Seq analysis and coverage plot

The raw sequencing reads obtained from the Chip-Seq analysis were first trimmed and filtered with Trim Galore! v0.4.4, and then aligned in single-end mode and searched against mm10 using Bowtie2 v2.2.9. The reads were then filtered using samtools to remove low-quality reads and unmapped reads. Duplicate reads were also filtered using Picard v2.16.0 MarkDuplicates. Peak calling was performed using MACS2 v2.1.1 with a *q*-value threshold of 0.05 and the --SPMR flag. The resulting bedgraph files were used to build a coverage plot using MACS2 v2.1.1 bdgcmp with the logLR method and a *P*-value of 1e−5.

Statistical analysis

Statistical analyses were conducted with Prism 6.0 software (GraphPad). An unpaired two-tailed *t*-test with a 95% confidence interval was used to calculate *P*-values. For retroviral transduction, SMARTA cell cotransfer, spleen chimera and BM chimera experiments, and a paired two-tailed *t*-test with the 95% confidence interval were used to calculate *P*-values.

RESULTS

Chromatin states of virus-specific T_{FH} and T_H1 cells in response to acute viral infection

In response to an acute viral infection, activated virus-specific $CD4^+$ T cells differentiate into either T_H1 or T_{FH} cells.[15,55,56] We first adoptively transferred LCMV-specific naïve SMARTA cells (expressing a transgenic T cell receptor specific for the LCMV glycoprotein epitope I-A^bGP66–77) into WT C57BL/6J recipients and subsequently infected the chimeric recipients with the LCMV Armstrong strain to investigate the potential regulatory regions involved in this bifurcated differentiation at the genome level. Then, we sorted virus-specific SMARTA T_{FH} cells and T_H1 cells from the SMARTA chimera mice on days 2, 5 and 8 after the infection (Supplementary Figure S1a–c) and subsequently performed an ATAC-Seq assay to measure the transposase-accessible chromatin.[40] We also sorted naïve SMARTA cells ($CD4^+CD25^-CD62L^+CD44^-$) as a control (Supplementary Figure S1d). QC of the ATAC-Seq libraries revealed the characteristic DNA fragment length distribution and the expected peak distribution across genomic features (Supplementary Figure S2a, b). With these high-quality libraries, we assessed the differences in chromatin-accessible regions (ChARs) and found that compared to naïve cells, dramatic changes in the numbers of ChARs emerged as early as day 2 postinfection in both virus-specific T_{FH} and T_H1 cells (Supplementary Figure S2c). Furthermore, chromatin-accessible patterns were discerned in T_{FH} and T_H1 cells, respectively, at different time points postinfection (Fig. 1a). The greatest differences in ChAR patterns were observed between T_{FH} and T_H1 cells at day 8 postinfection (Fig. 1a), reflecting the multistage differentiation of fully functional T_{FH} and T_H1 cells.[1] A ChAR-based PCA further revealed that T_{FH} and T_H1 cells started to enter two distinct $CD4^+$ T cell differentiation states on day 2 postinfection, and these differentiation trajectories continuously developed through the entire process (Fig. 1b).

K-means clustering of the differential peaks revealed four distinct areas, and the third and fourth clusters (gene lists are provided in Supplementary Tables S1 and S2) revealed opened ChARs that were specifically detected in T_H1 and T_{FH} cells, respectively (Fig. 1c), compared to naïve cells. Notably, when focusing on cluster 4, we found an array of T_{FH} lineage-associated gene loci that were enriched in this region, including *Bcl6*, *Tcf7*, *Id3*,[57] *Ascl2*,[58] *Cxcr5* and *Il21* (Fig. 1d). The T_H1-associated genes *Tbx21*, *Prdm1*, *Havcr2*, *Ccl3*, *Ccl4* and *Ccl5* were observed in cluster 3 (Fig. 1e). Further analysis of the ChARs for each individual gene locus revealed the stringent lineage-specific mode of chromatin accessibility; i.e., the chromatin accessibility of T_{FH}-associated genes was more prominent in T_{FH} cells than in T_H1 cells, and vice versa (Fig. 1d and e). Based on these results, chromatin remodeling is tightly associated with the T_{FH} but not T_H1 lineage commitment and differentiation in response to an acute viral infection.

Dynamic EZH2 expression and H3K27me3 modification in virus-specific T_{FH} cells

The EZH2-mediated H3K27me3 modification plays a critical role in chromatin remodeling.[59] Next, we sought to investigate the relationship between EZH2 expression and H3K27me3 modification during T_{FH} cell differentiation in response to an acute viral infection. We first adoptively transferred naïve SMARTA cells into WT C57BL/6J recipients, followed by an infection with the LCMV Armstrong strain. On day 2 after infection, we compared EZH2 expression and H3K27me3 modification between naïve ($CD44^{lo}CD25^-$), T_H1 ($CD25^{hi}CXCR5^-$) and T_{FH} ($CD25^{lo}CXCR5^+$) SMARTA cells. We observed the highest levels of EZH2 expression in T_{FH} cells compared to those in T_H1 and naïve cells, and T_H1 cells expressed a relatively higher level of EZH2 than the naïve cells (Fig. 2a). This phenotypic pattern was consistent with the levels of the EZH2-mediated H3K27me3 modification in T_{FH}, T_H1 and naïve SMARTA cells (Fig. 2b). Next, we analyzed the kinetics of EZH2 expression in T_{FH} SMARTA cells at different time points after infection and found that virus-specific T_{FH} cells rapidly increased EZH2 expression upon infection and reached a peak on day 2 postinfection (Fig. 2c). EZH2 expression then decreased to a comparable level to naïve cells on day 8 postinfection (Fig. 2c). Consistent with the EZH2 expression kinetics, the direct target of EZH2, H3K27me3, exhibited similar kinetics during T_{FH} cell differentiation (Fig. 2d).

The fate commitment of virus-specific T_{FH} cells occurs within the first 48 h after an acute viral infection. Therefore, the high expression of EZH2 in early differentiated T_{FH} cells on day 2 postinfection prompted us to examine whether the level of EZH2 expression correlated with T_{FH} cell commitment. For this purpose, on day 2 after infection, we divided SMARTA cells into three subsets, $EZH2^{hi}$, $EZH2^{inter}$ and $EZH2^{lo}$, according to their EZH2 expression levels and observed that the $EZH2^{hi}$ subset was much more poised to adopt the T_{FH} fate than the $EZH2^{inter}$ and $EZH2^{lo}$ subsets (Fig. 2e, f), while the opposite phenotype was observed during T_H1 differentiation (Fig. 2e–g). Compared to the $EZH2^{inter}$ and $EZH2^{lo}$ subsets, the $EZH2^{hi}$ subset expressed a significantly higher level of Bcl-6 (Fig. 2h), suggesting the enhanced propensity of this subset to become T_{FH} cells. Consistent with these findings, the extent of the H3K27me3 modification was also positively correlated with EZH2 expression and an early T_{FH} fate choice in SMARTA cells on day 2 after an acute viral infection (Fig. 2i–k). Collectively, high EZH2 expression and the associated H3K27me3 modification in activated virus-specific $CD4^+$ T cells preferentially drove them to differentiate into T_{FH} cells during the early response to acute viral infection, while the cells displaying low EZH2 and H3K27me3 levels were more prone to differentiate into T_H1 cells.

Role of EZH2 in early T_{FH} commitment during acute viral infection

Considering the positive correlation between the EZH2 expression level and T_{FH} commitment, we next investigated whether EZH2 is indeed essential for early T_{FH} differentiation upon acute viral infection. We crossed mice harboring *lox*P-flanked *Ezh2* alleles ($Ezh2^{fl/fl}$) with TCR-transgenic SMARTA mice that expressed the congenic marker CD45.1 to generate $Ezh2^{fl/fl}$ SMARTA mice (hereafter designated $Ezh2^{fl/fl}$ SM). Subsequently, we used a retroviral transduction system to overexpress codon-improved Cre recombinase (iCre) for the conditional deletion of EZH2 in virus-specific $Ezh2^{fl/fl}$ SM cells. Then, we transferred

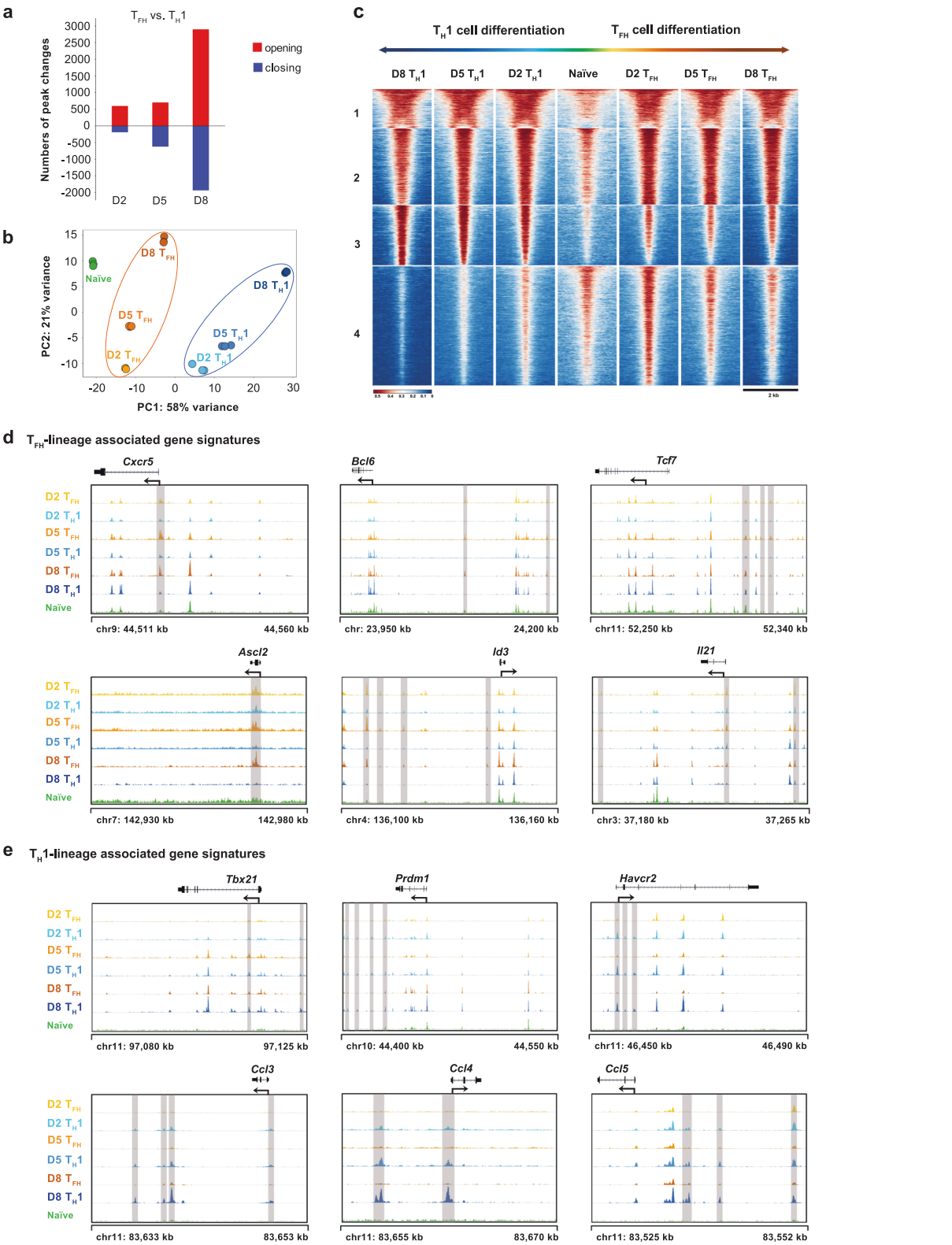

Fig. 1 Chromatin states of the virus-specific T_{FH} and T_H1 cells in response to an acute viral infection. **a** Numbers of chromatin peaks with differential accessibility (FDR < 0.05; FC > 4) between SMARTA T_{FH} cells and SMARTA T_H1 cells at the indicated time points after LCMV Armstrong infection. **b** PCA plot of the peak accessibilities in naïve SMARTA $CD4^+$ T cells, SMARTA T_{FH} cells (days 2, 5 and 8 postinfection) and SMARTA T_H1 cells (days 2, 5 and 8 postinfection). Each dot represents a replicate of the indicated group. **c** Chromatin accessibility heat map of differential peaks from **a**. Each row represents one of the 15,600 differential peaks that was center-aligned and extended upstream and downstream by 1 kb from the center. The peaks are *K*-means clustered. **d** ATAC-Seq signal profiles of T_{FH} lineage-associated gene loci. **e** ATAC-Seq signal profiles of T_H1 lineage-associated gene loci. Differential peaks are highlighted in gray (**d** and **e**). The data were obtained from one experiment with three biological replicates (pooled from at least five mice per group) (**a**–**e**)

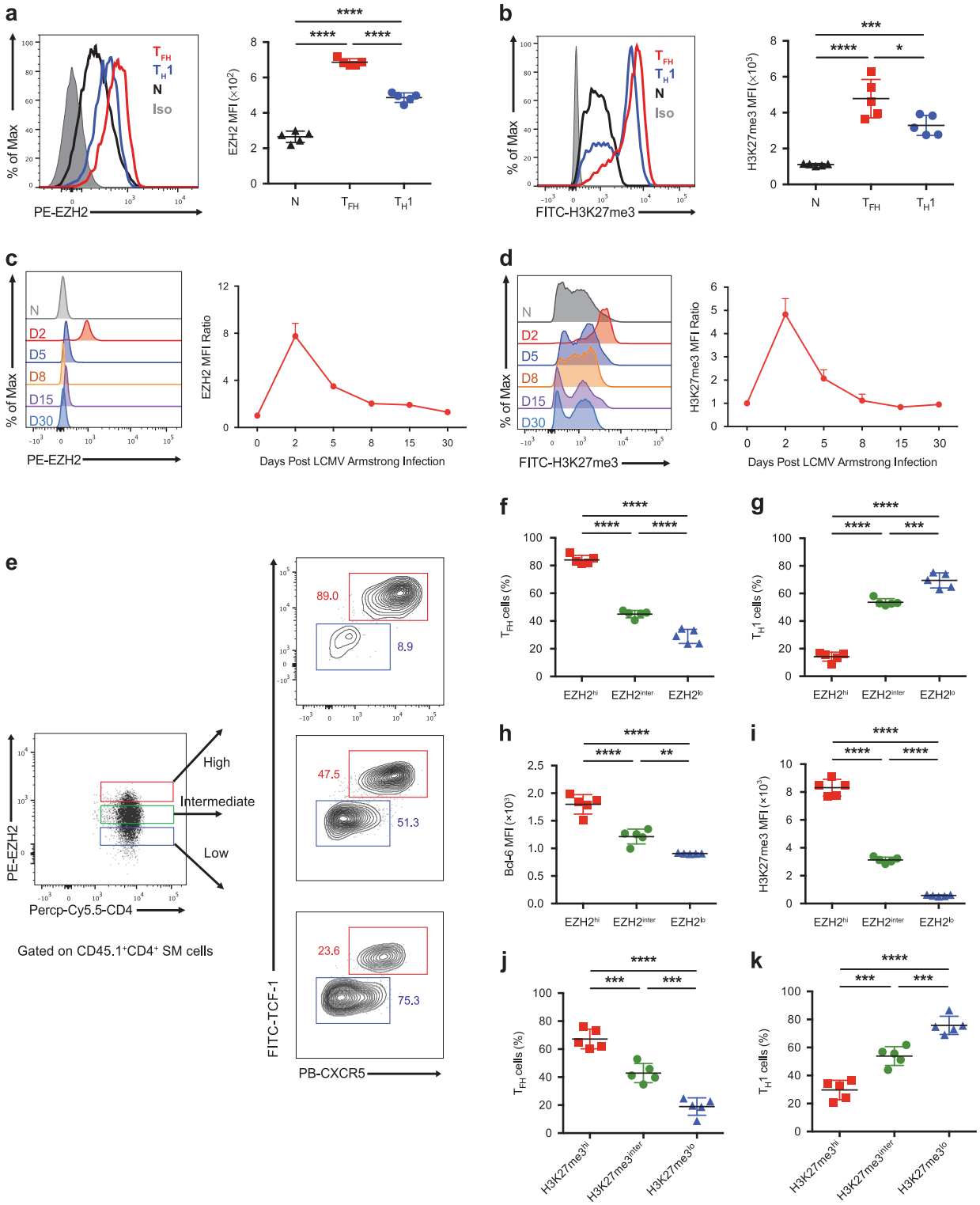

Fig. 2 Dynamic changes in EZH2 expression and the H3K27me3 modification in virus-specific T_{FH} cells. **a**, **b** Comparison of EZH2 (**a**) and H3K27me3 (**b**) levels between SMARTA T_{FH} cells ($CD25^{lo}CXCR5^{+}$) and SMARTA T_H1 cells ($CD25^{hi}CXCR5^{-}$) from the spleens of $CD45.2^{+}$ wild-type mice that underwent adoptive transfer of $CD45.1^{+}$ SMARTA cells and analyzed on day 2 after LCMV Armstrong infection and in naïve ($CD44^{lo}CD62L^{hi}$) SMARTA cells (N). **c**, **d** Flow cytometry analysis of EZH2 (**c**) and H3K27me3 (**d**) levels in T_{FH} cells derived from the mice listed in **a** on days 2, 5, 8, 15 and 30 after the LCMV Armstrong infection and in naïve SMARTA cells (N). The EZH2 or H3K27me3 mean fluorescence intensity (MFI) ratio at each time point was calculated as the MFI of T_{FH} cells / MFI of $CD4^{+}CD44^{lo}$ T cells in an identical mouse. **e** Flow cytometry analysis of the $EZH2^{hi}$, $EZH2^{inter}$ and $EZH2^{lo}$ subsets of T_{FH} cells and T_H1 cells from the mice shown in **a** on day 2 after the LCMV Armstrong infection. The proportions of T_{FH} cells and T_H1 cells and the MFI of Bcl-6 in each population are summarized in **f**, **g** and **h**, respectively. **i** The MFI of H3K27me3 in the $EZH2^{hi}$, $EZH2^{inter}$ and $EZH2^{lo}$ subsets of T_{FH} cells described in **e**. The proportions of T_{FH} cells (**j**) and T_H1 cells (**k**) among the $H3K27me3^{hi}$, $H3K27me3^{inter}$ and $H3K27me3^{lo}$ subsets of SMARTA cells from mice shown in **a** on day 2 after the LCMV Armstrong infection. $^{*}P < 0.05$, $^{***}P < 0.001$ and $^{****}P < 0.0001$ (unpaired two-tailed *t*-test). The data are representative of two independent experiments with at least four mice per group (**a**–**d** and **f**–**k**; error bars in **a**–**d** and **f**–**k** indicate the s.d.)

retrovirus-transduced and nontransduced *Ezh2*$^{fl/fl}$ SM cells or WT SM cells (*Ezh2*$^{+/+}$ SM) into naïve WT recipients that expressed the congenic marker CD45.2 and subsequently infected animals with the LCMV Armstrong strain (Fig. 3a). On day 2 after infection, we visualized the efficient deletion of EZH2 expression in *Ezh2*$^{fl/fl}$ SM cells overexpressing iCre (Supplementary Figure S3a). Notably, only 4.7% of iCre-expressing *Ezh2*$^{fl/fl}$ SM cells differentiated into CD25^{lo}CXCR5^{+} T_{FH} cells, whereas ~20% of virus-specific *Ezh2*$^{+/+}$ SM cells (with and without iCre recombinase) and *Ezh2*$^{fl/fl}$ SM cells (without iCre recombinase) were committed to the T_{FH} cell fate (Fig. 3b, c), highlighting the importance of EZH2 in T_{FH} fate determination.

We bred *Ezh2*$^{fl/fl}$ mice with SMARTA mice that transgenically expressed Cre recombinase downstream of the *Cd4* enhancer, promoter and silencer sequences (hereafter called *Ezh2*$^{fl/fl}$ SM-Cre) to further confirm the role of EZH2 in the early differentiation of virus-specific T_{FH} cells. We next mixed equal numbers of *Ezh2*$^{+/+}$ SM-Cre cells with *Ezh2*$^{fl/fl}$ SM-Cre cells and cotransferred these cells into WT recipients, which were subsequently infected with the LCMV Armstrong strain (Fig. 3d). On day 2 after infection, we validated the efficiency of *Ezh2* deletion in *Ezh2*$^{fl/fl}$ SM-Cre cells (Supplementary Figure S3b) and observed a remarkable reduction in the T_{FH} cell commitment of the *Ezh2*$^{fl/fl}$ SM-Cre cells compared to *Ezh2*$^{+/+}$ SM-Cre cells (Fig. 3e, f). Furthermore, we compared the expression levels of molecules that are closely associated with T_{FH} fate commitment, including TCF-1, Bcl-6, ICOS and CXCR5, between T_{FH} cells that differentiated from *Ezh2*$^{fl/fl}$ SM-Cre cells and *Ezh2*$^{+/+}$ SM-Cre cells (cells within the red circle in Fig. 3e). The levels of all examined molecules were substantially reduced in *Ezh2*$^{fl/fl}$ SM-Cre cell-derived T_{FH} cells compared to those in T_{FH} cells that differentiated from *Ezh2*$^{+/+}$ SM-Cre cells (Fig. 3g). Additionally, these phenotypes characterizing the early T_{FH} differentiation of *Ezh2*$^{fl/fl}$ SM-Cre cells in response to LCMV infection were largely confirmed to be the same cells upon an acute intracellular bacterial infection with a recombinant *L. monocytogenes* strain that expressed the LCMV glycoprotein epitope I-A^{b}GP61–80 (Supplementary Figure S3e–i).

Next, we investigated whether the inhibition of the EZH2-mediated H3K27me3 modification also led to defects in the T_{FH} cell commitment of virus-specific CD4^{+} T cells in response to a viral infection. For this purpose, we treated SMARTA cells with vehicle or the small molecule EPZ6438, which is a specific inhibitor of the H3K27me3 modification,[60] in vitro for 3 days and subsequently transferred these cells into WT recipients that were then infected with the LCMV Armstrong strain (Fig. 3h). Treatment with EPZ6438 efficiently reduced the levels of the H3K27me3 modification in SMARTA cells without affecting EZH2 expression (Supplementary Figure S3c and d). Notably, the inhibition of the H3K27me3 modification by the EPZ6438 treatment resulted in a substantial reduction in T_{FH} cell differentiation on day 2 postinfection compared to the T_{FH} commitment of vehicle-treated SMARTA cells (Fig. 3i, j). Furthermore, similar to results obtained using *Ezh2*$^{fl/fl}$ SM-Cre cell-derived T_{FH} cells (Fig. 3g), T_{FH} cells that differentiated from EPZ6438-treated SMARTA cells also exhibited lower expression of T_{FH} lineage-associated molecules, including TCF-1, Bcl-6, ICOS and CXCR5, compared to that of T_{FH} cells derived from vehicle-treated SMARTA cells (Fig. 3k). Taken together, these data validated the hypothesis that EZH2 expression and the subsequent H3K27me3 modification in virus-specific CD4^{+} T cells were important for early commitment to the T_{FH} cell fate in response to an acute viral infection.

Requirement for EZH2 expression in endogenous virus-specific T_{FH} cell differentiation

We bred *Ezh2*$^{fl/fl}$ mice with *Cd4*-Cre transgenic mice to further analyze the role of EZH2 in non-TCR transgenic, endogenous virus-specific T_{FH} cell differentiation. The resulting *Ezh2*$^{fl/fl}$*Cd4*-Cre mice conditionally lost EZH2 expression in their CD4^{+} T cell population (Supplementary Figure S4a). On day 8 after infection with the LCMV Armstrong strain, *Ezh2*$^{fl/fl}$*Cd4*-Cre mice exhibited a remarkable reduction in the virus-specific GP66–77 tetramer-positive CXCR5^{+}ICOS^{+} T_{FH} cell population in the spleen compared to that in *Ezh2*$^{fl/fl}$ control mice (Fig. 4a, b). Furthermore, the tetramer-positive T_{FH} cells from *Ezh2*$^{fl/fl}$*Cd4*-Cre mice exhibited decreased levels of T_{FH} differentiation-associated molecules, such as Bcl-6, TCF-1, PD-1 and CXCR5, compared to T_{FH} cells from *Ezh2*$^{fl/fl}$ control mice (Fig. 4c). These data revealed the effect of EZH2 deficiency on the T_{FH} differentiation of endogenous virus-specific CD4^{+} T cells, which were highly consistent with our observations in the *Ezh2*-null TCR-transgenic SMARTA cells shown in Fig. 3. Additionally, we compared the T_{FH} differentiation of bulk virus-activated Foxp3^{-}CD44^{hi} CD4^{+} T cells from *Ezh2*$^{fl/fl}$*Cd4*-Cre mice and *Ezh2*$^{fl/fl}$ control mice after LCMV infection. Similar to the impaired T_{FH} differentiation of GP66–77 tetramer-positive CD4^{+} T cells in *Ezh2*$^{fl/fl}$*Cd4*-Cre mice upon infection, the bulk-activated Foxp3^{-}CD44^{hi}CD4^{+} T cells from these mice also exhibited compromised CD44^{hi}CXCR5^{+}T_{FH} differentiation, as evidenced by the decreases in the proportion of T_{FH} cells, the T_{FH} to $T_{H}1$ ratio and the absolute T_{FH} number compared to that in *Ezh2*$^{fl/fl}$ control mice (Supplementary Figure S4b–d). As expected, T_{FH} cells lacking EZH2 expression displayed reduced levels of an array of T_{FH} lineage-associated proteins, including TCF-1, Bcl-6, PD-1 and ICOS (Supplementary Figure S4e).

Consistent with the defective T_{FH} differentiation caused by *Ezh2* deficiency in CD4^{+} T cells, *Ezh2*$^{fl/fl}$*Cd4*-Cre mice exhibited remarkably reduced frequencies and absolute numbers of PNA^{+}FAS^{+}GC B cells in the spleen on day 8 postinfection (Supplementary Figure S4f, g). The typical GC structure was also rarely observed in tissue sections of the spleens of *Ezh2*$^{fl/fl}$*Cd4*-Cre mice compared to sections from *Ezh2*$^{fl/fl}$ control mice, as revealed by a confocal microscopy analysis (Supplementary Figure S4h). Consistently, we noted less differentiation of B220^{lo}CD138^{hi} plasma cells in the spleens of *Ezh2*$^{fl/fl}$*Cd4*-Cre mice than that in the spleens of *Ezh2*$^{fl/fl}$ control mice (Supplementary Figure S4i and j). Given the defective T_{FH} differentiation and consequent scarcity of the GC B cell population in response to LCMV infection, *Ezh2*$^{fl/fl}$*Cd4*-Cre mice exhibited substantially reduced LCMV-specific IgG titers on days 8 and 90 postinfection compared with those of their *Ezh2*$^{fl/fl}$ counterparts (Supplementary Figure S4k).

We generated BM chimeras by mixing congenitally marked BM cells from *Ezh2*$^{fl/fl}$ERT2-Cre mice (expressing a fusion protein with a tamoxifen-sensitive estrogen receptor variant and Cre; CD45.2, 40%) with BM cells from WT mice (CD45.1, 60%) and subsequently injecting these mixtures into irradiated WT recipients to more precisely evaluate the role of cell-autonomous EZH2 in the mechanism regulating endogenous T_{FH} differentiation (Fig. 4d). After reconstitution, we first administered tamoxifen to efficiently delete EZH2 (Supplementary Figure S5a) and then infected these chimeric mice with the LCMV Armstrong strain. On day 8 after infection, a decreased percentage of Bcl-6^{hi}CXCR5^{+} T_{FH} cells was observed among GP66–77 tetramer-positive CD4^{+} T cells originating from *Ezh2*$^{fl/fl}$ ERT2-Cre mice compared with that of cells of WT origin (Fig. 4e, f). Significantly lower levels of TCF-1, Bcl6, PD-1 and CXCR5 were also detected in EZH2-deficient T_{FH} cells (*Ezh2*$^{fl/fl}$ ERT2-Cre) than those in control T_{FH} cells (WT) (Fig. 4g). We observed similar phenotypes in bulk T_{FH} cells from *Ezh2*$^{fl/fl}$ERT2-Cre and WT mice (Supplementary Figure S5b–e). Altogether, these data highlighted the importance of cell-intrinsic EZH2 in the mechanism regulating endogenous T_{FH} differentiation in response to an acute viral infection.

EZH2 is not required for the late differentiation and maintenance of virus-specific T_{FH} cells during an acute viral infection

We next determined the role of EZH2 in the late differentiation of T_{FH} cells during an acute infection. BM chimeras were generated by mixing BM cells from *Ezh2*$^{fl/fl}$ERT2-Cre mice (CD45.2, 40%) with

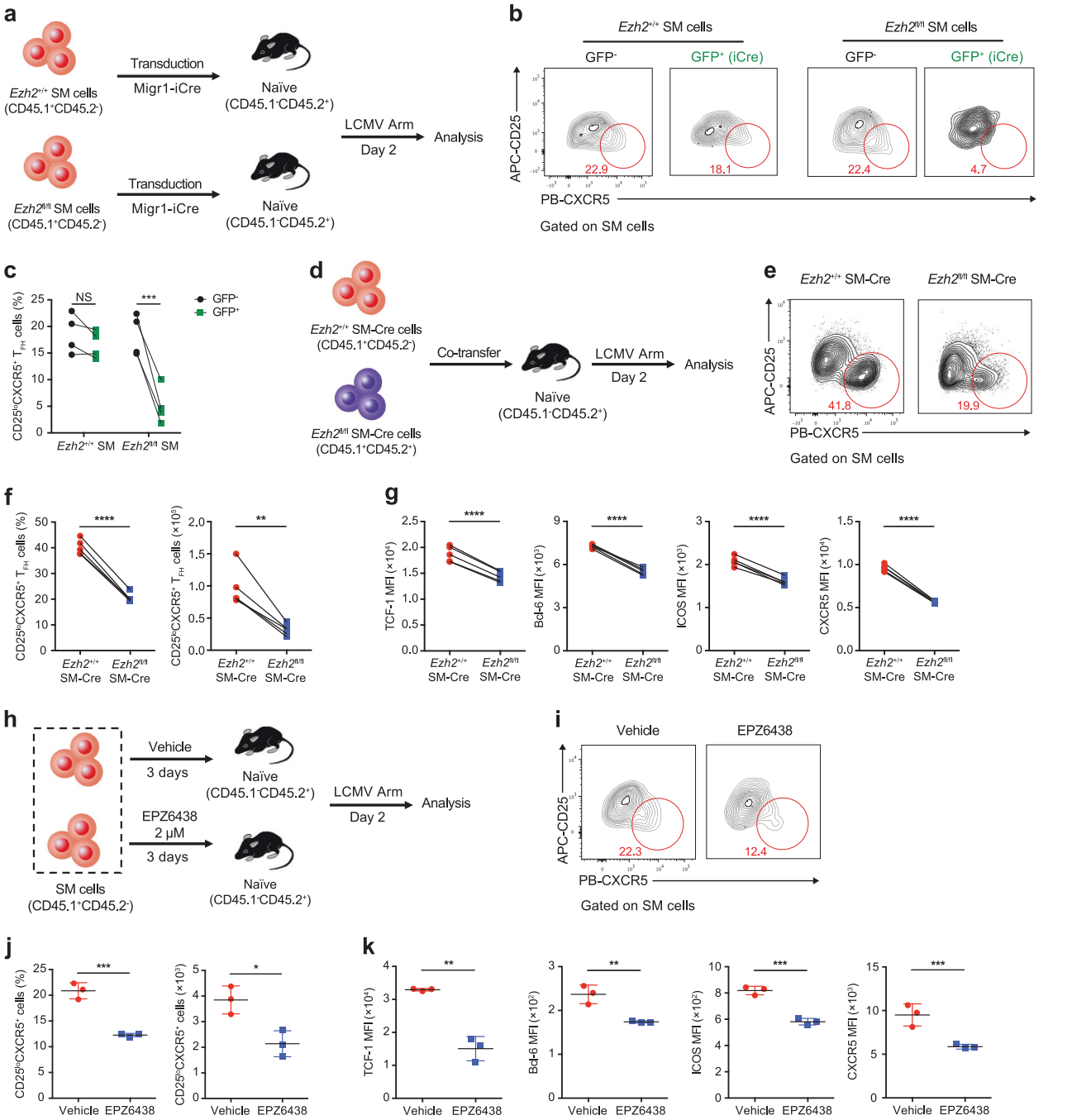

Fig. 3 Role of EZH2 in early T_{FH} commitment during an acute viral infection. **a** Experimental setup. A retrovirus overexpressing iCre was introduced into CD45.1$^+$*Ezh2*$^{+/+}$ SMARTA (SM) cells and CD45.1$^+$*Ezh2*$^{fl/fl}$ SM cells, which were transferred into CD45.2$^+$ WT recipients. Then, the recipients were infected with the LCMV Armstrong strain and analyzed on day 2 postinfection. **b** Flow cytometry analysis of *Ezh2*$^{+/+}$ and *Ezh2*$^{fl/fl}$ SM cells transduced with a retrovirus expressing iCre. The numbers adjacent to the outlined areas indicate the percentages of CD25^{lo}CXCR5$^+$ T_{FH} cells, which are summarized in **c**. **d** Experimental setup. *Ezh2*$^{+/+}$*Cd4*-Cre SMARTA cells (*Ezh2*$^{+/+}$ SM-Cre; CD45.1$^+$CD45.2$^-$) and *Ezh2*$^{fl/fl}$*Cd4*-Cre SMARTA cells (*Ezh2*$^{fl/fl}$ SM-Cre; CD45.1$^+$CD45.2$^+$) were cotransferred into WT recipients (CD45.1$^-$CD45.2$^+$), which were infected with the LCMV Armstrong strain and assessed on day 2 postinfection. **e** Flow cytometry analysis of *Ezh2*$^{+/+}$ SM-Cre and *Ezh2*$^{fl/fl}$ SM-Cre SMARTA cells. The numbers adjacent to the outlined areas indicate the percentages of CD25^{lo}CXCR5$^+$ T_{FH} cells, which are summarized in **f** (left panel). Total numbers of CD25^{lo}CXCR5$^+$ T_{FH} cells in **e** are presented (**f**, right panel). **g** Quantification of TCF-1, Bcl-6, ICOS and CXCR5 levels in the CD25^{lo}CXCR5$^+$ T_{FH} cells shown in **e**. **h** Experimental setup. After treatment with either EPZ6438 or vehicle for 3 days, CD45.1$^+$SMARTA cells were transferred into WT CD45.2$^+$ recipients that were subsequently infected with the LCMV Armstrong strain. The adoptively transferred SMARTA cells were analyzed on day 2 postinfection. **i** Flow cytometry analysis of EPZ6438-treated and vehicle-treated SMARTA cells. The numbers adjacent to the outlined areas indicate the proportions of CD25^{lo}CXCR5$^+$ T_{FH} cells, which are summarized in **j** (left panel). Total numbers of CD25^{lo}CXCR5$^+$ T_{FH} cells analyzed in **i** are presented in **j** (right panel). **k** Quantification of TCF-1, Bcl-6, ICOS and CXCR5 levels in the CD25^{lo}CXCR5$^+$ T_{FH} cells shown in **j**. NS not significant; *$P < 0.05$, **$P < 0.01$, ***$P < 0.001$ and ****$P < 0.0001$ (paired two-tailed *t*-test (**c**, **f** and **g**) or unpaired two-tailed *t*-test (**j** and **k**)). The data are representative of two independent experiments with at least three mice (**c**, **f**, **g**, **j** and **k**) per group (error bars in **j** and **k** indicate the s.d.)

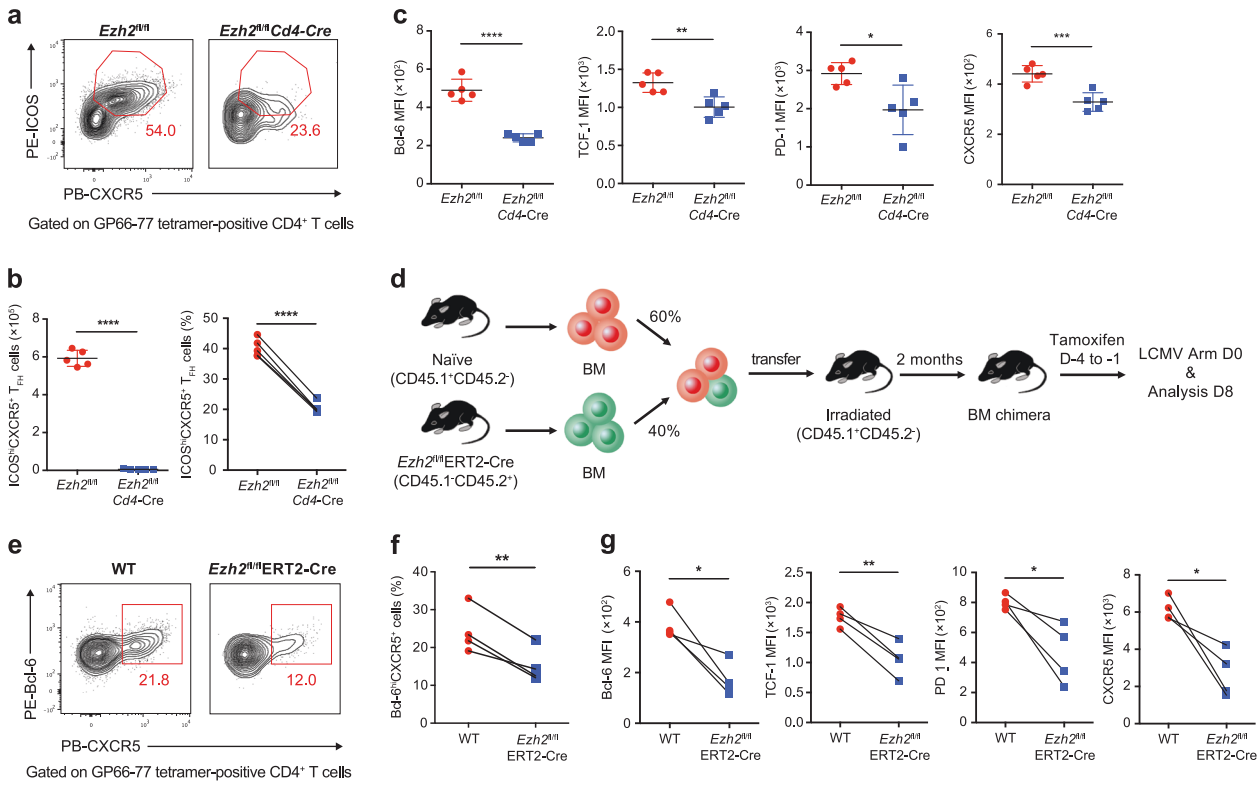

Fig. 4 Requirement for EZH2 expression in endogenous virus-specific T_{FH} cell differentiation. **a** Flow cytometry analysis of GP66–77 tetramer-positive $CD4^+$ T cells in the spleens of *Ezh2*$^{fl/fl}$*Cd4*-Cre mice and *Ezh2*$^{fl/fl}$ mice on day 8 after LCMV Armstrong infection. The numbers adjacent to the outlined areas indicate the proportions of ICOS^{hi}CXCR5$^+$ T_{FH} cells. **b** The percentage (left panel) and number (right panel) of ICOS^{hi}CXCR5$^+$ T_{FH} cells in **a**. **c** Quantification of Bcl-6, TCF-1, PD-1 and CXCR5 levels in the ICOS^{hi}CXCR5$^+$ T_{FH} cells shown in **a**. **d** Setup of the BM chimera experiment. Irradiated CD45.1$^+$ WT recipients underwent the adoptive transfer of CD45.1$^+$ WT BM cells (60%) and CD45.2$^+$ *Ezh2*$^{fl/fl}$ERT2-Cre BM cells (40%). Two months after reconstitution, the recipients were treated with tamoxifen and then infected with the LCMV Armstrong strain. **e** Flow cytometry analysis of GP66–77 tetramer-positive $CD4^+$ T cells in the spleens of recipient mice shown in **d** on day 8 after the LCMV Armstrong infection. The numbers adjacent to the outlined areas indicate the proportions of Bcl-6^{hi}CXCR5$^+$ T_{FH} cells, which are summarized in **f**. **g** Quantification of Bcl-6, TCF-1, PD-1 and CXCR5 levels in the Bcl-6^{hi}CXCR5$^+$ T_{FH} cells shown in **e**. NS not significant; $^*P < 0.05$, $^{**}P < 0.01$, $^{***}P < 0.001$ and $^{****}P < 0.0001$ (unpaired two-tailed *t*-test (**b** and **c**) or paired two-tailed *t*-test (**f** and **g**)). The data are representative of two independent experiments with at least four mice (**b**, **c**, **f** and **g**) per group (error bars in **b** and **c** indicate the s.d.)

BM cells from WT mice (CD45.1, 60%) and subsequently injecting the mixtures into irradiated WT recipients (Fig. 5a). After reconstitution, these chimeric mice were initially infected with the LCMV Armstrong strain and then administered tamoxifen from days 4 to 7 after infection to induce the deletion of EZH2 (Fig. 5b). Notably, we observed comparable virus-specific Bcl-6^{hi}CXCR5$^+$ T_{FH} cell proportions between cells from *Ezh2*$^{fl/fl}$ ERT2-Cre and WT mice (Fig. 5c, d). Consistent with the intact late T_{FH} cell differentiation, the levels of molecules related to T_{FH} cell differentiation, including Bcl-6, PD-1 and ICOS, were also similar between cells from *Ezh2*$^{fl/fl}$ ERT2-Cre and WT mice (with the exception of a reduction in TCF-1 expression) (Fig. 5e). BM chimeric mice were infected with LCMV Armstrong and then administered tamoxifen from days 9 to 12 to ablate EZH2 expression and further determine whether EZH2 is required for the maintenance of virus-specific T_{FH} cells (Fig. 5f). On day 60 postinfection, normal virus-specific T_{FH} cell proportions were observed in the absence of EZH2 (Fig. 5g–i). Hence, EZH2 is not required for the late differentiation and the maintenance of virus-specific T_{FH} cells in response to an acute viral infection, suggesting a specific effect on early T_{FH} fate commitment.

EZH2 remodels T_{FH} lineage-associated chromatin accessibility during viral infection

We investigated the impact of the EZH2 deficiency on chromatin state changes in virus-specific T_{FH} cells to obtain an understanding of the epigenetic modifications mediated by EZH2 to regulate T_{FH} differentiation. Therefore, we analyzed ATAC-Seq libraries (Supplementary Figure S6a, b) generated from WT T_{FH} cells, EZH2-KO T_{FH} cells and naïve $CD4^+$ T cells. Compared to naïve $CD4^+$ cells, both WT T_{FH} and KO T_{FH} cells showed significant changes in opening and closing peaks in the genome, suggesting the presence of different chromatin states (Fig. 6a). This finding was clearly revealed in the PCA plot (Fig. 6b): the KO T_{FH} cells showed a chromatin state that differed from WT T_{FH} cells and naïve T cells. The EZH2 deficiency resulted in the remodeling of a cluster of specific gene loci that are closely associated with T_{FH} differentiation, which were almost identical to the loci identified in Fig. 1d, including *Bcl6*, *Tcf7*, *Id3*, *Ascl2*, *Cxcr5*, *Icos*, *Il21* and *Sh2d1a*[1] (Fig. 6c). Notably, these loci were less open in *Ezh2* KO T_{FH} cells than those in WT T_{FH} cells (Fig. 6c). Because the EZH2-directed H3K27me3 modification is generally associated with a closed state of chromatin accessibility, we further probed whether these loci were marked by the H2K27me3 modification. Therefore, we sorted virus-specific T_{FH} cells and T_H1 cells from the SMARTA chimeric mice on day 2 after the LCMV Armstrong infection and naïve $CD4^+$ T cells ($CD4^+CD25^-CD62L^+CD44^-$) from naïve mice and subsequently performed H3K27me3 ChIP-Seq experiments. Strikingly, T_{FH}-associated genes (e.g., *Bcl6*, *Tcf7*, *Id3* and *Cxcr5*) were selectively marked by the EZH2-associated H3K27me3 modification in T_H1 cells, but not in T_{FH} cells, during the bifurcated $CD4^+$ T cell differentiation (Fig. 6d). Thus, although EZH2 functions as a chromatin repressor, it appeared to rewind the chromatin states of certain T_{FH}-associated genes to favor T_{FH} differentiation.

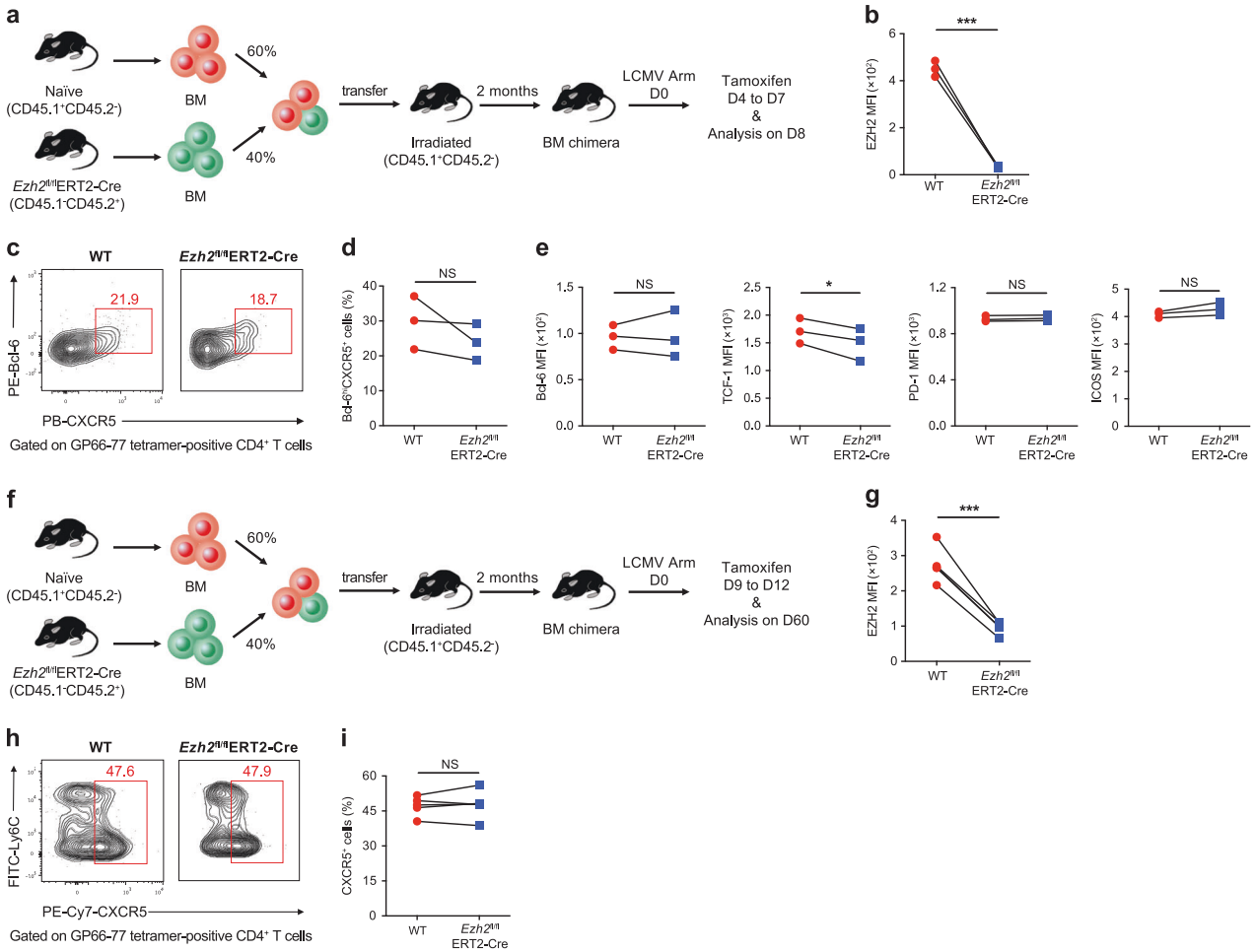

Fig. 5 EZH2 is not essential for the late differentiation and maintenance of virus-specific T_{FH} cells during an acute viral infection. **a** Setup of the BM chimera experiment. Irradiated CD45.1$^+$ WT recipients underwent adoptive transfer of CD45.1$^+$ WT BM cells (60%) and CD45.2$^+$ *Ezh2*$^{fl/fl}$ERT2-Cre BM cells (40%). Two months after reconstitution, the recipients were infected with LCMV Armstrong, followed by the administration of tamoxifen from days 4 to 7 after infection and an analysis on day 8. **b** Expression of EZH2 in virus-specific Bcl6^{hi}CXCR5$^+$ T_{FH} cells from the BM chimeric WT and *Ezh2*$^{fl/fl}$ERT2-Cre mice shown in **a**. **c** Flow cytometry analysis of GP66–77 tetramer-positive CD4$^+$ T cells in the spleens of the chimeras described in **a** on day 8 after the LCMV Armstrong infection. Numbers adjacent to outlined areas indicate the percentage of Bcl-6^{hi}CXCR5$^+$ T_{FH} cells, which were summarized in **d**. **e** Levels of Bcl-6, TCF-1, PD-1 and ICOS in the Bcl-6^{hi}CXCR5$^+$ T_{FH} cells shown in **c**. **f** The BM chimeras described in **a** were infected with LCMV Armstrong, treated with tamoxifen on days 9 to 12 after infection and analyzed on day 60. **g** Quantification of EZH2 expression in virus-specific CXCR5$^+$ T_{FH} cells originating from BM chimeric WT and *Ezh2*$^{fl/fl}$ERT2-Cre mice shown in **f**. **h** Flow cytometry of GP66–77 tetramer-positive CD4$^+$ T cells in the spleens of the chimeras described in **f** on day 60 after the LCMV Armstrong infection. Numbers adjacent to outlined areas indicate the percentage of CXCR5$^+$ T_{FH} cells, which were summarized in **i**. NS not significant; *$P < 0.05$ and ***$P < 0.001$ (paired two-tailed *t*-test (**b**, **d**, **e**, **g** and **i**)). The data are representative of two independent experiments with at least three mice (**b**, **d**, **e**, **g**, **h** and **i**) per group

Bcl-6 overexpression rescues compromised H3K27me3 modification-induced T_{FH} cell differentiation

Consistent with the reduced accessibility of important ChARs in T_{FH} cells caused by the EZH2 deficiency (Fig. 6c), the expression of the corresponding genes was substantially reduced, as revealed by microarray analyses (Fig. 7a). In addition to the genes analyzed in Fig. 6c (including *Bcl6*, *Tcf7*, *Id3*, *Ascl2*, *Cxcr5*, *Icos*, *Il21* and *Sh2d1a*), we also observed the downregulation of the mRNA levels of several other T_{FH} differentiation-associated genes, such as *Tcf3*,[57] *Cd40lg*,[7] *Pdcd1*, *Egr3*,[61] *Lef1*, *Batf* and *Cd28* (ref. [62]) (Fig. 7a). We further confirmed our discoveries by performing reverse-transcription quantitative PCR (RT-PCR) assays (Fig. 7b). These results raised the possibility that EZH2-mediated H3K27 trimethylation increases the chromatin accessibility, primarily at T_{FH}-differentiation-associated genes, which then induce a favorable transcription program directing T_{FH} lineage commitment.

Bcl-6 is the master regulator of T_{FH} cell differentiation.[16–18] Because virus-specific CD4$^+$ T cells with abundant Bcl-6 and EZH2 expression tend to differentiate into the T_{FH} cell fate (Fig. 2f–h), and lower levels of the Bcl-6 protein (Figs. 3g, k, 4c and g) and mRNA (Fig. 7a, b) and reduced chromatin accessibility (Fig. 6c) are observed in EZH2-deficient T_{FH} cells, we hypothesized that the impaired T_{FH} cell commitment observed in the absence of EZH2 is potentially driven by compromised Bcl-6 expression and that Bcl6 overexpression might rescue the defective T_{FH} differentiation of activated virus-specific CD4$^+$ T cells with decreased EZH2 activities. Naïve SMARTA cells were transduced with a retrovirus encoding Bcl-6 and then treated with vehicle or the H3K27me3 inhibitor EPZ6438 in vitro for 3 days to evaluate this hypothesis. After treatment, these cells were adoptively transferred into WT recipients, which were immediately infected with the LCMV Armstrong strain (Fig. 7c). Consistent with published studies,[16–18] forced Bcl-6 expression biased vehicle-treated SMARTA cells to T_{FH} cell differentiation on day 5 postinfection (Fig. 7d, e; 42.5% vs. 76.2%). Meanwhile, a substantial reduction in the T_{FH} cell differentiation of nontransduced SMARTA cells was observed in

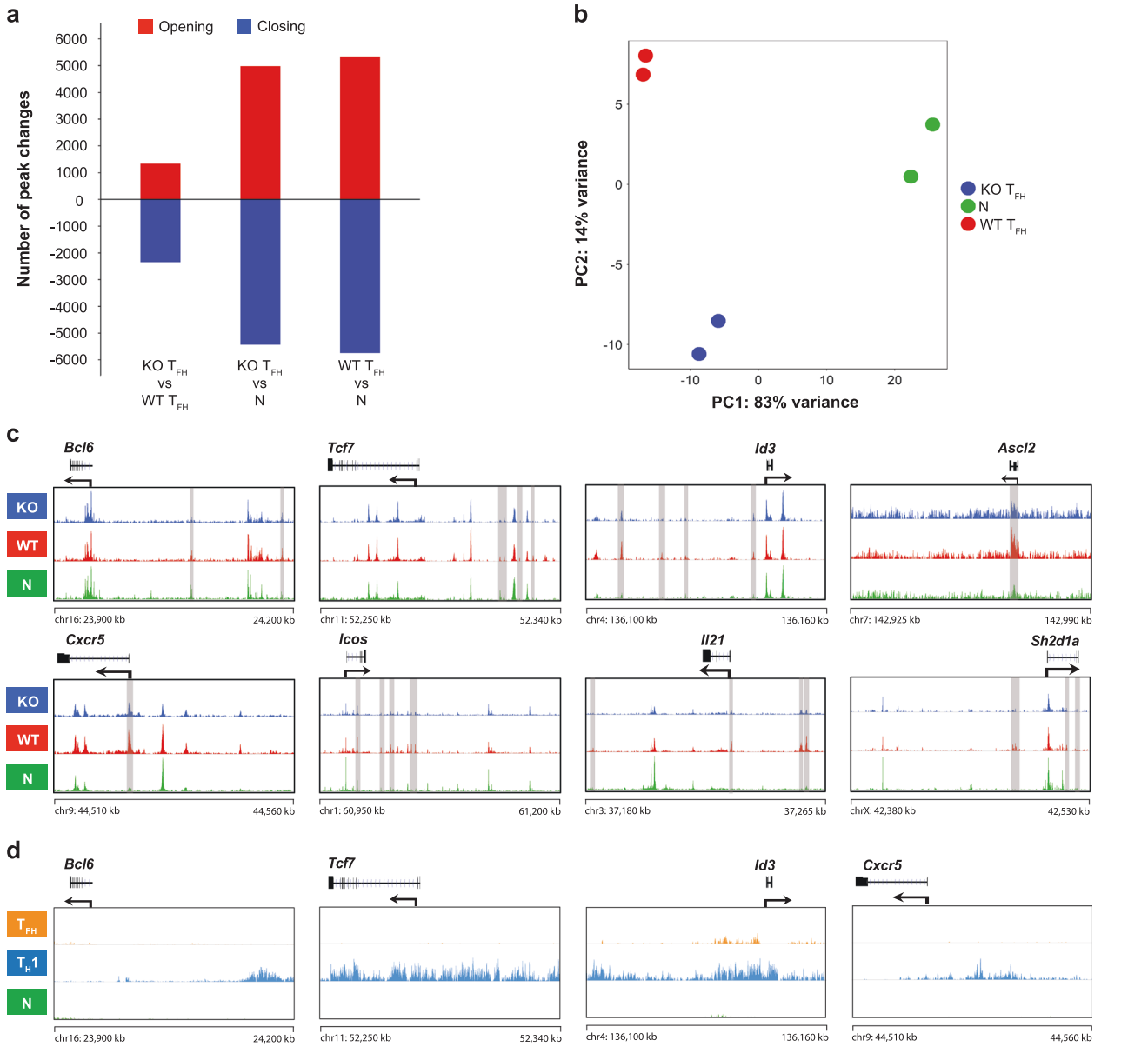

Fig. 6 Role of EZH2 in the remodeling of T_{FH} lineage-associated chromatin accessibility during viral infection. **a** Numbers of chromatin peaks with differential accessibility (FDR < 0.05; FC > 1.5) in naïve $CD4^+$ T cells (N), WT T_{FH} cells and KO T_{FH} cells. **b** PCA plot of the peak accessibilities in naïve $CD4^+$ T cells (green), WT T_{FH} cells (red) and KO T_{FH} cells (blue). Each dot represents a replicate of the group. **c** ATAC-Seq signal profiles of T_{FH} lineage-associated gene loci in naïve $CD4^+$ T cells (N), WT T_{FH} cells and KO T_{FH} cells. **d** Tracks of H3K27me3 ChIP-Seq data from T_{FH} lineage-associated gene loci in naïve $CD4^+$ T cells (N), T_{FH} cells and T_H1 cells. The data were obtained from two independent experiments with one biological replicate (pooled from at least five mice per group) in each experiment (**a**–**c**) and from one experiment with one biological replicate (**d**)

the EPZ6438-treated group compared to that in the vehicle-treated group (Fig. 7d, e; 42.5% vs. 19.9%), consistent with our aforementioned data (Fig. 3j). Strikingly, Bcl-6 overexpression in EPZ6438-treated SMARTA cells restored the T_{FH} cell commitment to a similar level as the forced Bcl-6 expression-amplified T_{FH} cell commitment in the vehicle group (Fig. 7d, e; 76.2% vs. 67.9%). Taken together, the EZH2-associated H3K27me3 modification is a crucial positive determinant of Bcl-6 expression, which further directs T_{FH} cell differentiation.

DISCUSSION

During the initial phase of an acute viral infection, activated virus-specific $CD4^+$ T cells differentiate into either T_H1 or T_{FH} cells.[15,55,56] Bcl-6 is required to specify the T_{FH} fate choice,[16–18] and Blimp-1 antagonizes this effect by suppressing Bcl-6 expression and Bcl-6-mediated transcriptional activity.[16] Thus, the Bcl-6–Blimp-1 balance coordinates the early T_{FH} commitment. The preserved and elevated TCF-1 expression in activated virus-specific $CD4^+$ T cells induces Bcl-6 expression but inhibits Blimp-1 expression, and thus, it plays a critical role in guiding the T_{FH} commitment pathway.[15] Currently, little is known about the epigenetic mechanism that stabilizes these TF networks during early T_{FH} fate determination. In this study, we defined a distinct chromatin state in virus-specific T_{FH} cells compared to virus-specific T_H1 cells in response to an acute infection. Importantly, early fate-committed T_{FH} cells exhibited higher expression of the histone methyltransferase EZH2 in response to an acute viral infection and

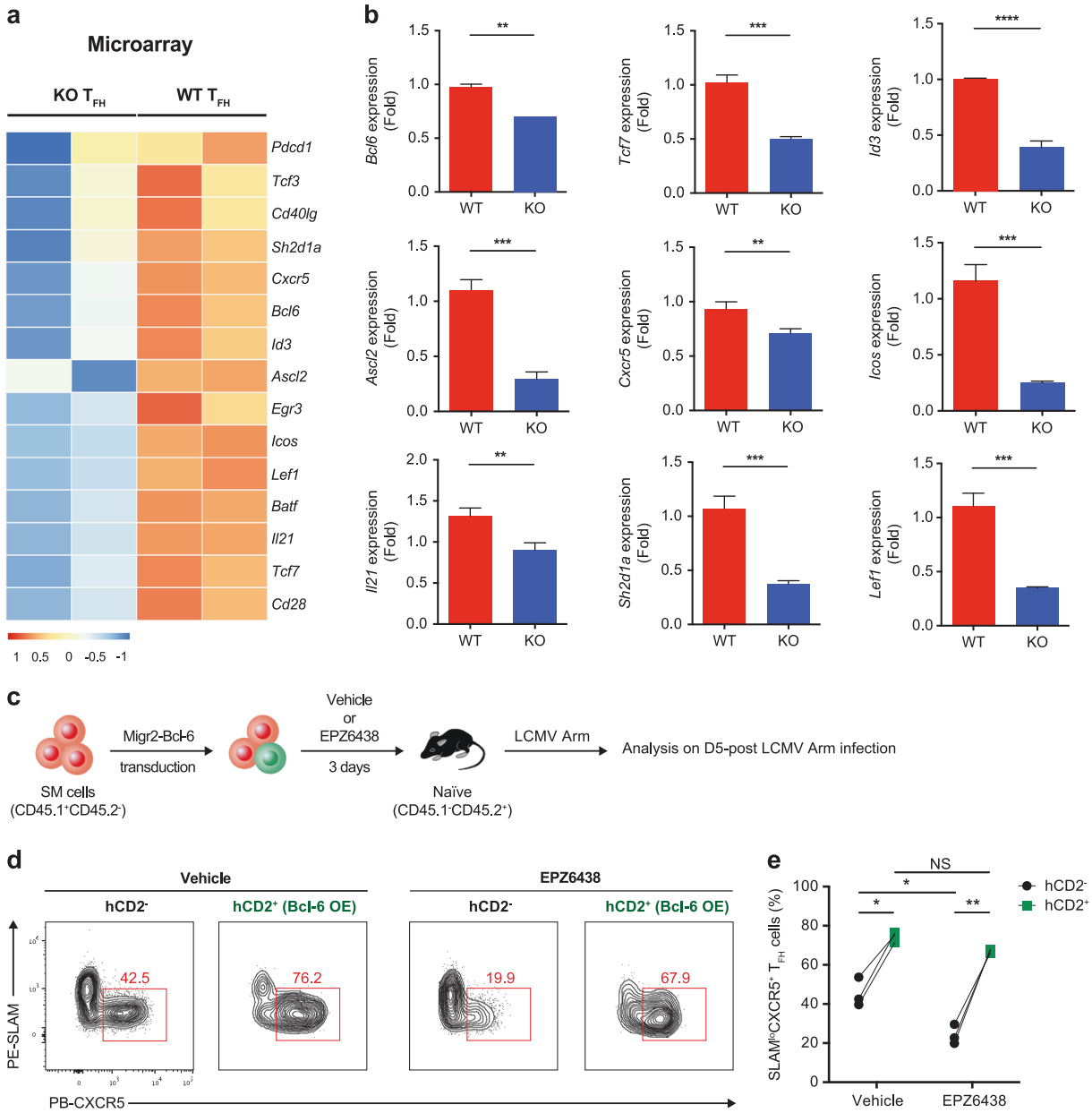

Fig. 7 Bcl-6 overexpression rescues compromised H3K27me3 modification-induced T_{FH} cell differentiation. **a** Heat map of the canonical T_{FH} lineage-associated genes in WT T_{FH} cells and EZH2 KO T_{FH} cells based on data obtained from the microarray analysis. **b** Quantitative RT-PCR of selected genes in **a** (normalized to their expression in WT T_{FH} cells). **c** Experimental setup. After treatment with either EPZ6438 or vehicle for 3 days, CD45.1$^+$SMARTA (SM) cells transduced with an empty retrovirus or retroviral vector overexpressing *Bcl6* were transferred into WT CD45.2$^+$ recipients that were subsequently infected with LCMV Armstrong. The adoptively transferred SM cells were analyzed on day 5 postinfection. **d** Flow cytometry analysis of vehicle/EPZ6438-treated SM cells that were transduced with (hCD2$^+$) or without (hCD2$^-$) a retrovirus expressing Bcl-6. The numbers adjacent to the outlined areas indicate the percentages of SLAM^{lo}CXCR5$^+$ T_{FH} cells, which are summarized in **e**. NS not significant; $^*P < 0.05$, $^{**}P < 0.01$, $^{***}P < 0.001$ and $^{****}P < 0.0001$ (unpaired two-tailed *t*-test (**b**); paired two-tailed *t*-test (**e**)). The data were obtained from one experiment with two biological replicates pooled from at least ten mice per group (**a**), are representative of two independent experiments with three technical replicates pooled from at least ten mice per group (**b**) or are representative of two independent experiments with at least three mice (**e**) per group (**b**; error bars indicate the s.d.)

accordingly increased levels of the H3K27me3 modification compared with that of their T_H1 counterparts. The ablation of EZH2 by genetic deletion in virus-specific CD4$^+$ T cells substantially reduced the early T_{FH} commitment by disrupting the T_{FH}-specific chromatin state. Specifically, EZH2 is required for the stabilization of chromatin accessibility and transcription pattern of *Bcl6*, which is essential for the T_{FH} fate commitment. Thus, our results highlighted the importance of EZH2, a widely recognized chromatin repressor, in the priming of T_{FH} cell fate commitment by reinforcing Bcl-6 expression in activated T_{FH} precursors.

T_{FH} differentiation is characterized as a stepwise process:[1] early fate commitment (2 days after an acute infection, occurring at the T–B border), maturation (3–4 days after an acute infection, occurring in B-cell follicle and pre-GC) and memory formation (~1–2 months after an acute infection). In our study, the chromatin identity of virus-specific T_{FH} cells was discerned from virus-specific T_H1 cells within the first 2 days after viral infection. In particular, chromatin remodeling of a cluster of T_{FH} lineage differentiation-associated genes, including *Bcl6*, *Tcf7*, *Id3*, *Ascl2*, *Cxcr5*, *Icos*, *Il21* and *Sh2d1a*, was observed in virus-specific T_{FH} cells. This distinct

chromatin pattern is maintained throughout the differentiation process and maximized on day 8 postinfection, indicating a progressive mechanism regulating the chromatin states of T_{FH} cells in response to an acute infection.

TCR stimulation is crucial for the effective induction of EZH2 expression in $CD4^+$ T cells.[33,63] The enhanced strength and duration of the interaction between TCR and pMHC favors T_{FH} differentiation,[64] which may partially explain the elevated EZH2 expression levels observed in T_{FH} cells compared to those of their T_H1 counterparts following an acute viral infection. During T_{FH} differentiation, EZH2 expression spikes within 2 days after infection and then decreases to the baseline level that is comparable to naive $CD4^+$ T cells. This dynamic pattern of EZH2 expression is further evidenced by a crucial role for EZH2 in the early commitment but not late differentiation or memory maintenance of T_{FH} cells. Strikingly, the ablation of EZH2 in early committed T_{FH} cells leads to the expression of a cluster of T_{FH} lineage differentiation-associated genes with less chromatin accessibility, including *Bcl6*, *Tcf7*, *Id3*, *Ascl2*, *Cxcr5*, *Icos*, *Il21* and *Sh2d1a*. In this regard, TCR-trigged EZH2 seems to imprint a T_{FH}-associated chromatin pattern in T_{FH} precursors at an early stage of the bifurcated T_{FH} and T_H1 differentiation. The EZH2-mediated H3K27me3 modification generally leads to a closed state of chromatin accessibility, but our results identified an essential role for this epigenetic modification in promoting the chromatin accessibility of a cluster of T_{FH}-associated genes in T_{FH} cells. These effects appeared to be indirect, since we did not observe the deposition of H3K27me3 marks at these T_{FH}-associated loci in T_{FH} cells. Alternatively, EZH2 and its associated H3K27me3 modification may orchestrate other chromatin modifications that directly target specific loci of these genes to promote T_{FH} differentiation. Further studies will be required to identify potential candidate chromatin modifiers downstream of EZH2 and to dissect the underlying regulatory mechanisms.

EZH2 has been reported to negatively regulate the differentiation of an array of effector T_H cell subsets, including T_H1, T_H2 and T_H17 cells.[36–38] These suppressive effects are likely mediated by the EZH2-driven H3K27me3 modifications that directly target and silence a variety of genes required for the differentiation of these cell subsets, including lineage-specifying TFs and/or cytokines, such as *Tbx21*, *Gata3* and *Ifng*, *Il13* and *Il17*. In sharp contrast to its negative role in modulating the differentiation of other T_H lineages, our study revealed that EZH2 instructed the early commitment to T_{FH} cell differentiation by stabilizing a cluster of T_{FH} cell lineage-associated genes, including *Bcl6*. Consistent with our results, a newly published study[65] revealed a requirement for EZH2 in governing T_{FH} cell differentiation by integrating phosphorylation-dependent *Bcl6* activation and H3K27me3-dependent repression of p19Arf. Therefore, EZH2 regulates T_H differentiation in a cell-type-specific manner.

In conclusion, the present study is the first to define a distinct chromatin state in early committed T_{FH} cells that is maintained throughout the acute viral infection. The histone methyltransferase EZH2 is involved in this process and plays a critical role in priming the early T_{FH} cell fate commitment by promoting the stabilization of T_{FH} lineage-specific chromatin pattern. These findings provide valuable insights into strategies targeting EZH2 to improve vaccine efficacy and may aid in the development of novel therapeutic strategies for diseases associated with aberrant T_{FH} differentiation.

Accession codes: GEO: ATAC-Seq data and H3K27me3 ChIP-Seq data, GSE110722; microarray data, GSE110458.

ACKNOWLEDGEMENTS

We thank R. Ahmed (Emory University) for providing the SMARTA transgenic mice and retroviral vectors; CapitalBio Corporation (Beijing, China) for performing microarray experiments and data analysis; the Core Facility Center of the Third Military Medical University for performing cell sorting; the University of Chicago Research Computing Center for supporting this study; and Dr. Yifei Hu (University of Chicago) and Dr. Chufan Cai (University of Chicago) for performing the ATAC-Seq and ChIP-Seq experiments. This study was supported by grants from the National Key Research Development Plan (No. 2016YFA0502202 to L.Y.), the Open Research Fund of State Key Laboratory of Veterinary Biotechnology (No. SKLVBF2018XX to L. Ye), the National Natural Science Foundation of China (No. 31825011 to L.Y.; No. 31800742 to Q.T.; No. 31700774 to L. Xu and No. 31470870 to X.Z.) and Chicago Biomedical Consortium with support from the Searle Funds at The Chicago Community Trust (to J.H.).

AUTHOR CONTRIBUTIONS

X.C., J.W., X.W., J.G., Z.P., Q.T., L.Xu., Z.Li., Y.H., Q.H., P.W., M.X., L.Xi., S.T., Z.Liu., L.H, J.T, R. H., S.T. and Z.L. performed the experiments. G.C. and M.C. analyzed the ATAC-Seq data and microarray data. L.Y. designed the study, analyzed the data and wrote the paper with assistance from J.H., X.C., G.C., L.W., X.Z., Y.W. and B.S.; and L.Y., B.Z. and J. H. supervised the study.

ADDITIONAL INFORMATION

The online version of this article (https://doi.org/10.1038/s41423-019-0219-z) contains supplementary material.

Competing interests: The authors declare no competing interests.

REFERENCES

1. Crotty, S. Follicular helper CD4 T cells (TFH). *Annu. Rev. Immunol.* **29**, 621–663 (2011).
2. Victora, G. D. & Nussenzweig, M. C. Germinal centers. *Annu. Rev. Immunol.* **30**, 429–457 (2012).
3. Vinuesa, C. G., Linterman, M. A., Yu, D. & MacLennan, I. C. Follicular helper T cells. *Annu. Rev. Immunol.* **34**, 335–368 (2016).
4. Linterman, M. A. et al. IL-21 acts directly on B cells to regulate Bcl-6 expression and germinal center responses. *J. Exp. Med.* **207**, 353–363 (2010).
5. Reinhardt, R. L., Liang, H. E. & Locksley, R. M. Cytokine-secreting follicular T cells shape the antibody repertoire. *Nat. Immunol.* **10**, 385–393 (2009).
6. Wang, Y. et al. Germinal-center development of memory B cells driven by IL-9 from follicular helper T cells. *Nat. Immunol.* **18**, 921–930 (2017).
7. Liu, D. et al. T-B-cell entanglement and ICOSL-driven feed-forward regulation of germinal centre reaction. *Nature* **517**, 214–218 (2015).
8. Good-Jacobson, K. L. et al. PD-1 regulates germinal center B cell survival and the formation and affinity of long-lived plasma cells. *Nat. Immunol.* **11**, 535–542 (2010).
9. Breitfeld, D. et al. Follicular B helper T cells express CXC chemokine receptor 5, localize to B cell follicles, and support immunoglobulin production. *J. Exp. Med.* **192**, 1545–1552 (2000).
10. Kim, C. H. et al. Subspecialization of CXCR5+T cells: B helper activity is focused in a germinal center-localized subset of CXCR5+T cells. *J. Exp. Med.* **193**, 1373–1381 (2001).
11. Schaerli, P. et al. CXC chemokine receptor 5 expression defines follicular homing T cells with B cell helper function. *J. Exp. Med.* **192**, 1553–1562 (2000).
12. Ansel, K. M., McHeyzer-Williams, L. J., Ngo, V. N., McHeyzer-Williams, M. G. & Cyster, J. G. In vivo-activated CD4 T cells upregulate CXC chemokine receptor 5 and reprogram their response to lymphoid chemokines. *J. Exp. Med.* **190**, 1123–1134 (1999).
13. Gunn, M. D. et al. A B-cell-homing chemokine made in lymphoid follicles activates Burkitt's lymphoma receptor-1. *Nature* **391**, 799–803 (1998).
14. Crotty, S. T follicular helper cell differentiation, function, and roles in disease. *Immunity* **41**, 529–542 (2014).
15. Xu, L. et al. The transcription factor TCF-1 initiates the differentiation of T(FH) cells during acute viral infection. *Nat. Immunol.* **16**, 991–999 (2015).
16. Johnston, R. J. et al. Bcl6 and Blimp-1 are reciprocal and antagonistic regulators of T follicular helper cell differentiation. *Science* **325**, 1006–1010 (2009).
17. Nurieva, R. I. et al. Bcl6 mediates the development of T follicular helper cells. *Science* **325**, 1001–1005 (2009).
18. Yu, D. et al. The transcriptional repressor Bcl-6 directs T follicular helper cell lineage commitment. *Immunity* **31**, 457–468 (2009).
19. Choi, Y. S., Eto, D., Yang, J. A., Lao, C. & Crotty, S. Cutting edge: STAT1 is required for IL-6-mediated Bcl6 induction for early follicular helper cell differentiation. *J. Immunol.* **190**, 3049–3053 (2013).
20. Nurieva, R. I. et al. Generation of T follicular helper cells is mediated by interleukin-21 but independent of T helper 1, 2, or 17 cell lineages. *Immunity* **29**, 138–149 (2008).

21. Schmitt, N. et al. Human dendritic cells induce the differentiation of interleukin-21-producing T follicular helper-like cells through interleukin-12. *Immunity* **31**, 158–169 (2009).
22. Betz, B. C. et al. Batf coordinates multiple aspects of B and T cell function required for normal antibody responses. *J. Exp. Med.* **207**, 933–942 (2010).
23. Bollig, N. et al. Transcription factor IRF4 determines germinal center formation through follicular T-helper cell differentiation. *Proc. Natl Acad. Sci. USA* **109**, 8664–8669 (2012).
24. Auderset, F. et al. Notch signaling regulates follicular helper T cell differentiation. *J. Immunol.* **191**, 2344–2350 (2013).
25. Stone, E. L. et al. ICOS coreceptor signaling inactivates the transcription factor FOXO1 to promote Tfh cell differentiation. *Immunity* **42**, 239–251 (2015).
26. Choi, Y. S. et al. LEF-1 and TCF-1 orchestrate T(FH) differentiation by regulating differentiation circuits upstream of the transcriptional repressor Bcl6. *Nat. Immunol.* **16**, 980–990 (2015).
27. Wu, T. et al. TCF1 is required for the T follicular helper cell response to viral infection. *Cell Rep.* **12**, 2099–2110 (2015).
28. Steinke, F. C. & Xue, H. H. From inception to output, Tcf1 and Lef1 safeguard development of T cells and innate immune cells. *Immunol. Res.* **59**, 45–55 (2014).
29. Busslinger, M. & Tarakhovsky, A. Epigenetic control of immunity. *Cold Spring Harb. Perspect. Biol.* **6**, pii: a019307 (2014).
30. Karantanos, T., Chistofides, A., Barhdan, K., Li, L. & Boussiotis, V. A. Regulation of T cell differentiation and function by EZH2. *Front. Immunol.* **7**, 172 (2016).
31. Margueron, R. & Reinberg, D. The Polycomb complex PRC2 and its mark in life. *Nature* **469**, 343–349 (2011).
32. Schuettengruber, B., Chourrout, D., Vervoort, M., Leblanc, B. & Cavalli, G. Genome regulation by polycomb and trithorax proteins. *Cell* **128**, 735–745 (2007).
33. DuPage, M. et al. The chromatin-modifying enzyme Ezh2 is critical for the maintenance of regulatory T cell identity after activation. *Immunity* **42**, 227–238 (2015).
34. Jacob, E., Hod-Dvorai, R., Schif-Zuck, S. & Avni, O. Unconventional association of the polycomb group proteins with cytokine genes in differentiated T helper cells. *J. Biol. Chem.* **283**, 13471–13481 (2008).
35. Tong, Q. et al. Ezh2 regulates transcriptional and posttranslational expression of T-bet and promotes Th1 cell responses mediating aplastic anemia in mice. *J. Immunol.* **192**, 5012–5022 (2014).
36. Tumes, D. J. et al. The polycomb protein Ezh2 regulates differentiation and plasticity of CD4(+) T helper type 1 and type 2 cells. *Immunity* **39**, 819–832 (2013).
37. Yang, X. P. et al. EZH2 is crucial for both differentiation of regulatory T cells and T effector cell expansion. *Sci. Rep.* **5**, 10643 (2015).
38. Zhang, Y. et al. The polycomb repressive complex 2 governs life and death of peripheral T cells. *Blood* **124**, 737–749 (2014).
39. Shen, H. et al. Recombinant Listeria monocytogenes as a live vaccine vehicle for the induction of protective anti-viral cell-mediated immunity. *Proc. Natl Acad. Sci. USA* **92**, 3987–3991 (1995).
40. Buenrostro, J. D., Giresi, P. G., Zaba, L. C., Chang, H. Y. & Greenleaf, W. J. Transposition of native chromatin for fast and sensitive epigenomic profiling of open chromatin, DNA-binding proteins and nucleosome position. *Nat. Methods* **10**, 1213–1218 (2013).
41. Martin, M. Cutadapt removes adapter sequences from high-through sequencing reads. *EMBnet J.* **17**, 10–12 (2011).
42. Langmead, B. & Salzberg, S. L. Fast gapped-read alignment with Bowtie 2. *Nat. Methods* **9**, 357–359 (2012).
43. Li, H. et al. The Sequence Alignment/Map format and SAMtools. *Bioinformatics* **25**, 2078–2079 (2009).
44. Adey, A. et al. Rapid, low-input, low-bias construction of shotgun fragment libraries by high-density in vitro transposition. *Genome Biol.* **11**, R119 (2010).
45. Ramirez, F. et al. deepTools2: a next generation web server for deep-sequencing data analysis. *Nucleic Acids Res.* **44**, W160–W165 (2016).
46. Zhang, Y. et al. Model-based analysis of ChIP-Seq (MACS). *Genome Biol.* **9**, R137 (2008).
47. Quinlan, A. R. & Hall, I. M. BEDTools: a flexible suite of utilities for comparing genomic features. *Bioinformatics* **26**, 841–842 (2010).
48. Li, Q. H., Brown, J. B., Huang, H. Y. & Bickel, P. J. Measuring repoducibility of high-throughput experiments. *Ann. Appl. Stat.* **5**, 1752–1779 (2011).
49. Zhu, L. J. et al. ChIPpeakAnno: a Bioconductor package to annotate ChIP-seq and ChIP-chip data. *BMC Bioinformatics* **11**, 237 (2010).
50. Love, M. I., Huber, W. & Anders, S. Moderated estimation of fold change and dispersion for RNA-seq data with DESeq2. *Genome Biol.* **15**, 550 (2014).
51. Robinson, J. T. et al. Integrative genomics viewer. *Nat. Biotechnol.* **29**, 24–26 (2011).
52. Ye, L., Zeng, R., Bai, Y., Roopenian, D. C. & Zhu, X. Efficient mucosal vaccination mediated by the neonatal Fc receptor. *Nat. Biotechnol.* **29**, 158–163 (2011).
53. Rasheed, M. A. et al. Interleukin-21 is a critical cytokine for the generation of virus-specific long-lived plasma cells. *J. Virol.* **87**, 7737–7746 (2013).
54. He, R. et al. Follicular CXCR5- expressing CD8(+) T cells curtail chronic viral infection. *Nature* **537**, 412–428 (2016).
55. Hale, J. S. et al. Distinct memory CD4+ T cells with commitment to T follicular helper- and T helper 1-cell lineages are generated after acute viral infection. *Immunity* **38**, 805–817 (2013).
56. Marshall, H. D. et al. Differential expression of Ly6C and T-bet distinguish effector and memory Th1 CD4(+) cell properties during viral infection. *Immunity* **35**, 633–646 (2011).
57. Shaw, L. A. et al. Id2 reinforces TH1 differentiation and inhibits E2A to repress TFH differentiation. *Nat. Immunol.* **17**, 834–843 (2016).
58. Liu, X. et al. Transcription factor achaete-scute homologue 2 initiates follicular T-helper-cell development. *Nature* **507**, 513–518 (2014).
59. Chen, T. & Dent, S. Y. Chromatin modifiers and remodellers: regulators of cellular differentiation. *Nat. Rev. Genet.* **15**, 93–106 (2014).
60. Knutson, S. K. et al. Durable tumor regression in genetically altered malignant rhabdoid tumors by inhibition of methyltransferase EZH2. *Proc. Natl Acad. Sci. USA* **110**, 7922–7927 (2013).
61. Ogbe, A. et al. Early growth response genes 2 and 3 regulate the expression of Bcl6 and differentiation of T follicular helper cells. *J. Biol. Chem.* **290**, 20455–20465 (2015).
62. Weber, J. P. et al. ICOS maintains the T follicular helper cell phenotype by down-regulating Kruppel-like factor 2. *J. Exp. Med.* **212**, 217–233 (2015).
63. Dobenecker, M. W. et al. Signaling function of PRC2 is essential for TCR-driven T cell responses. *J. Exp. Med.* **215**, 1101–1113 (2018).
64. Fazilleau, N., McHeyzer-Williams, L. J., Rosen, H. & McHeyzer-Williams, M. G. The function of follicular helper T cells is regulated by the strength of T cell antigen receptor binding. *Nat. Immunol.* **10**, 375–384 (2009).
65. Li, F. et al. Ezh2 programs TFH differentiation by integrating phosphorylation-dependent activation of Bcl6 and polycomb-dependent repression of p19Arf. *Nat. Commun.* **9**, 5452 (2018).